Dalton Transactions

Accepted Manuscript

ROYAL SOCIETY OF CHEMISTRY

www.rsc.org/dalton

Cite this: DOI: 10.1039/c0xx00000x

www.rsc.org/xxxxxx

ARTICLE TYPE

Mediator-Free Direct Z-scheme Photocatalytic System: $BiVO_4$/g-C_3N_4 Organic-Inorganic Hybrid Photocatalyst with Highly Efficient Visible-Light-Induced Photocatalytic Activity

Na Tian[a], Hongwei Huang[a]*, Ying He [a], Yuxi Guo [a], Tieriu Zhang [b], Yihe Zhang [a]*

Received (in XXX, XXX) Xth XXXXXXXXX 20XX, Accepted Xth XXXXXXXXX 20XX
DOI: 10.1039/b000000x

We disclose the fabrication of a mediator-free direct Z-scheme photocatalyst system $BiVO_4$/g-C_3N_4 by using a mixed-calcination method based on more reliable interfacial interaction. The facet coupling occurred between the g-C_3N_4 (002) and $BiVO_4$ (121) was revealed by X-ray diffraction (XRD), X-ray photoelectron spectroscopy (XPS) and transmission electron microscope (TEM). The crystal structure and optical property of the as-prepared samples have also been characterized by fourier-transform infrared (FTIR), scanning electron microscopy (SEM) and UV-vis diffuse reflectance spectra (DRS) in details. The photocatalytic experiments indicated that the $BiVO_4$/g-C_3N_4 composite photocatalysts display a significantly enhanced photocatalytic activity pertaining to RhB degradation and photocurrent generation (PC) compared to the pristine $BiVO_4$ and g-C_3N_4. This remarkably improved photocatalytic performance should be attributed to the fabrication of a direct Z-scheme system of $BiVO_4$/g-C_3N_4, which can result in a more efficient separation of photoinduced charge carriers than band-band transfer, thus endowing it with the much more powerful oxidation and reduction capability, as confirmed by the photoluminescence (PL) spectra and electrochemical impedance spectra (EIS). The Z-scheme mechanism of $BiVO_4$/g-C_3N_4 heterostructure was verified by a series of combined techniques, including the active species trapping experiments, NBT transformation and terephthalic acid photoluminescence probing technique (TA-PL) over $BiVO_4$/g-C_3N_4 composites and the pristine samples. The present work not only furthered the understanding of mediator-free Z-scheme photocatalysis, but also shed new light on the design of heterostructural photocatalysts with high-performance.

1. Introduction

As a green and potential technology, semiconductor photocatalysis plays a vital role in the aspects of environmental protection and solar energy conversion.[1-7] Numerous attention have been paid toward the design of novel visible-light-responsive photocatalysts so as to maximize the utilization of the natural sunlight in the visible region (λ > 420 nm), which accounts for the largest proportion of the solar spectrum. Construction of heterostructures between two semiconductors is considered to be an effective method to promote the photocatalytic activity. Nowadays, the Z-scheme principled photocatalyst has attracted considerable attention due to its much stronger redox capacity than band-band transfer photocatalyst. The more negative CB and more positive VB potentials in Z-scheme photocatalyst separately endow the photogenerated electrons and holes with strong reduction and oxidation ability, thereby exhibiting significantly improved photocatalytic performance than the single component.[8,9] For instance, the photocatalytic activity through the direct Z-scheme principle transfer is obviously higher than that by band-band transfer mechanism in the visible-light-responsive Ag@AgBr/g-C_3N_4 composite photocatalyst.[6] Other Z-scheme photocatalysts also largely prolong the lifetime of photoexcited carriers and exhibit highly enhanced photocatalytic activity than the two individuals. The Z-scheme systems are usually obtained by coupling two different photocatalysts combined with an appropriate intermediate or mediator (e.g. noble metals Ag and Au),[10-13] which suffer from many drawbacks, such as low stability, high cost, etc. Compared with the mediator-containing ternary Z-scheme system, the mediator-free direct Z-scheme photocatalytic system only consisting of two components exhibits high stability, economic feasibility, etc, thus possessing the more promising practical application.[14-17]

As a promising candidate photocatalyst for organic pollutant removal and hydrogen production, graphite-like carbon nitride (g-C_3N_4) exhibits relatively high photocatalytic activity under visible-light irradiation due to its rapid separation of photoinduced charge carriers.[18-20] The very negative conduction band (-1.13 eV) of g-C_3N_4 enables a strong reduction power of the electrons (e^-) in the conduction band (CB). Nevertheless,

there are still some shortcomings for the g-C_3N_4 utilization in photocatalysis process, such as the limited visible-light absorption below 450 nm, and small specific surface area.[21,22] Recently, continuous efforts have been made to improve the photocatalytic performance of g-C_3N_4. Among which, combining g-C_3N_4 with other appropriate semiconductors to construct heterostructures can effectively promote the separation rate of photoexcitated charge carriers. $BiVO_4$ is a visible-light-responsive photocatalyst with a narrow band gap of 2.40 eV, which has been admitted as a potential visible-light photocatalyst.[23-25] However, the photogenerated e^- and h^+ can be quickly decay via recombination,[26] resulting in relatively low photocatalytic activity of $BiVO_4$. Therefore, it limits the practical applications of $BiVO_4$ in photocatalytic degradation of pollutants. Consequently, it is an urgent strategy to enhance the efficiency of charge carries separation rate and improve the visible-light photocatalytic activity of $BiVO_4$.

After energy level analysis, we found that the gap between the CB of g-C_3N_4 and the CB of $BiVO_4$ is much larger than that between the CB of $BiVO_4$ and the VB of g-C_3N_4. It may lead to that the photoinduced electrons in the CB of $BiVO_4$ transfer to the VB of g-C_3N_4 rapidly, which leaves rich electrons in the CB of g-C_3N_4 and holes in the VB of $BiVO_4$ to participate in the redox process, thus may resulting in a mediator-free direct Z-scheme photocatalytic system. Herein, we successfully prepared the direct Z-scheme photocatalyst system of $BiVO_4$/g-C_3N_4 by employing a mixed-calcination method, which may provide a more strong and reliable interfacial interaction between g-C_3N_4 and $BiVO_4$. The coupling between g-C_3N_4 and $BiVO_4$ happens on the (002) and (121) facets of g-C_3N_4 and $BiVO_4$, respectively. The photochemical activity of the $BiVO_4$/g-C_3N_4 was monitored via photocatalytic decomposition of the Rhodamine B (RhB) and photocurrent generation under visible-light irradiation ($\lambda > 420$ nm). The direct Z-scheme system of $BiVO_4$/g-C_3N_4 leads to a high efficiency separation of photogenerated electrons and holes, thus a highly improved photocatalytic activity. It was demonstrated by the active species trapping experiments, NBT transformation and terephthalic acid photoluminescence probing technique (TA-PL). It will be a generalized strategy to design other mediator-free direct Z-scheme photocatalysts with high-performance.

2. Experimental Section

2.1 Synthesis of heterostructured $BiVO_4$/g-C_3N_4 photocatalyst

The chemicals used in this study were of analytical grade without further purification. The g-C_3N_4 was synthesized via a calcination treatment of 5 g melamine in a corundum crucible without a cover in nitrogen.[23,26] The crucible containing melamine was put into tube furnace and heated at 520℃ for 4h. After cooling to room temperature, the yellow g-C_3N_4 product was obtained.

Pure $BiVO_4$ was prepared by a hydrothermal method as following. First of all, 0.005 mol of $Bi(NO_3)_3$•$5H_2O$ was completely dissolved in 20 mL of HNO_3 (2 M) to form solution A. Second, 0.005 mol of NH_4VO_3 was dissolved in 10 mL of 2 M NaOH solution to form solution B. Then, solution B was dropwise added into solution A to form a yellow mixture suspension. NaOH solution (1 M) was used to adjust the pH value to 7 of the obtained suspension and following by 30 min vigorously stirring. Then, move the resultant mixture to a 100 mL Teflon-lined stainless steel autoclave. The sealed autoclave was maintained at 180 ℃ for 12 h and afterwards cooling to room temperature naturally. After that, a yellow $BiVO_4$ powder was obtained with centrifugation, washed with water repeatedly, and finally dried in a vacuum oven.

The $BiVO_4$/g-C_3N_4 composites were obtained according to the following procedure. In a typical synthesis of $BiVO_4$/g-C_3N_4 with the molar ratio 1:9, 0.009 mol of g-C_3N_4 and 0.001 mol of $BiVO_4$ were mixed and ground thoroughly for 5 min. After that, the mixture was calcined at 400℃ for 4 h to obtain the 1:9 $BiVO_4$/g-C_3N_4 photocatalyst. Other $BiVO_4$/g-C_3N_4 photocatalysts (2:8, 3:7, 4:6, 5:5 $BiVO_4$/g-C_3N_4) were prepared by the same processes, only the molar ratio of $BiVO_4$ to g-C_3N_4 were different. The pristine $BiVO_4$ and g-C_3N_4 were handled by the same method to ensure that they are under the same conditions.

2.2 Characterization

X-ray diffraction (XRD) analysis was employed to evaluate the phase structure of the as-prepared photocatalysts on a XRD-3 powder diffraction instrument with monochromatized Cu Kα radiation (λ= 1.5406 nm) at a setting of 40 kV and 40 mA, and the scanning rate and range were 0.02° (2θ)/s and 10-70°, respectively. A Bruker spectrometer was used to achieve the fourier-transform infrared (FTIR) spectra at a frequency range of 4000-500 cm^{-1}. Scanning electron microscopy (SEM) on a FEI Quanta 250 FEG instrument was applied to examine the general morphology of the photocatalysts. And a S-4300 transmission electron microscope (TEM, Hitachi) was employed to obtain the morphology and microstructure. The specific surface area was collected through Brumauer-Emmett-Teller (BET) method by N_2 adsorption (ASAP 2460, Micromeritics, USA). UV-vis diffuse reflectance spectra (DRS) of the samples were recorded on a Cary 5000 (America Varian) spectrophotometer. The surface properties of the photocatalysts were obtained by X-ray photoelectron spectroscopy (XPS) on a Thermo ESCALAB 250 instrument (USA) operating at 150 W with Al Kα X-ray irradiation. The photoluminescence (PL) spectra were measured on a Hitachi F-4600 fluorescence spectrophotometer to investigate the recombination rate of electrons and holes.

2.3 Photocatalytic evaluation

As a common organic pollutant, RhB was employed to evaluate the photocatalytic activities of the as-prepared photocatalysts under visible-light ($\lambda > 420$ nm) degradation illuminated by a 500 W xenon lamp. 50 mg of the powder photocatalysts were dropped into quartz tubes which were containing 50 mL RhB solution (1×10^{-5} mol/L), respectively. Then, the above solution was ultrasonic dispersion for 10 min and stirred for 30 min in dark to achieve an adsorption-desorption equilibrium between the photocatalyst powder and RhB. Turn on the light and the photocatalytic reaction systems were exposed to visible light irradiation. At the same intervals, 3 mL of the mixture were taken out to centrifuge tubes, and the catalysts were removed out of the suspensions (4500 r/min, 5 min). The centrifuged solution was analyzed by recording the maximum absorption band (554 nm)

and UV-vis spectra were recorded by Shimadzu UV-5500PC spectrophotometer (produced by Shanghai Wuxiang Company).

2.4 Active species trapping and $\bullet O_2^-$ and •OH quantification experiments

Tert-butyl alcohol (TBA), 1, 4-benzoquinone (BQ) and disodium ethylenediaminetetraacetate (EDTA) were added in order to investigate the main active species, such as hydroxyl radicals (•OH), superoxide radical ($\bullet O_2^-$) and holes (h^+) produced during the photoreaction process.[10,27,28] NBT[17] (2.5×10^{-5} mol/L) was used to detect the amount of $\bullet O_2^-$ generated from g-C_3N_4, $BiVO_4$, 3:7 $BiVO_4$/g-C_3N_4 and mechanically mixed 3:7 $BiVO_4$/g-C_3N_4. The production of $\bullet O_2^-$ was quantitatively analyzed by detecting the concentration of NBT with Shimadzu UV-5500PC spectrophotometer. To determine the amount of •OH producing from g-C_3N_4, $BiVO_4$, 3:7 $BiVO_4$/g-C_3N_4 and mechanically mixed 3:7 $BiVO_4$/g-C_3N_4, TA[29,30] (5×10^{-4} M in a 2×10^{-3} M NaOH solution) was used as a probe molecule to react with •OH generating a highly fluorescent product 2-hydroxyterephthalic acid, whose concentration can reflect the yield of •OH measured by a Hitachi F-4600 fluorescence spectrophotometer.

2.5 Photoelectrochemical measurements experiments

The electrochemical experiments, including photocurrent response and electrochemical impedance spectra (EIS) of the samples as visible-light on and off, were conducted on a CHI660C electrochemical workstation (Chenhua Instrument Corporation, Shanghai). The $BiVO_4$/g-C_3N_4 film electrodes on ITO served as the working electrode, while a carbon electrode and a platinum maturated calomel electrode (SCE) were employed as the counter electrode and reference electrode, respectively. A xenon lamp with a power of 500 W acted as visible-light source, and 0.1 M Na_2SO_4 was used as the supporting electrolyte. The working voltage of the $BiVO_4$/g-C_3N_4 electrode was 0 V. And the whole process of the measurement was conducted in air at room temperature.

3. Results and discussion

3.1. Characterization

XRD analysis was applied to survey and evaluate the phase structure of the samples. Fig. 1a shows the XRD patterns of g-C_3N_4, $BiVO_4$ and $BiVO_4$/g-C_3N_4 with different molar ratios. For the pure g-C_3N_4, it can be clearly seen that the two distinct diffraction peaks at 27.40° and 13.04°correspond to the (002) and (100) diffraction planes, respectively, revealing that the diffraction peaks of g-C_3N_4 were in good agreement with the tetragonal phase of g-C_3N_4 (JCPDS 87-1526).[31,32] Pure $BiVO_4$ shows a series of narrow and sharp diffraction peaks, which can be identified as the monoclinic phase of $BiVO_4$ (JCPDS 14-0688).[33,34] For $BiVO_4$/g-C_3N_4 samples, it can be observed that the characteristic peaks of g-C_3N_4 gradually appeared with the increase of the g-C_3N_4 content. Thus, the XRD patterns of $BiVO_4$/g-C_3N_4 samples demonstrated that the characteristic diffraction peaks consisted of both g-C_3N_4 and $BiVO_4$, reflecting existence of the two phases.

Fig. 1b shows the FTIR spectra of g-C_3N_4, $BiVO_4$ and $BiVO_4$/g-C_3N_4 composites. In the spectrum of pure $BiVO_4$, the peak at 742 cm^{-1} can be attributed to the ν_3 asymmetric stretching vibration of the VO_4 unit ν_3 (VO_4), and that at 842 cm^{-1} corresponded to the ν_1 symmetric stretching vibration of the VO_4 unit ν_1 (VO_4).[35,36] The absorption bands of pure g-C_3N_4 sample indicated the typical molecular structure of g-C_3N_4. The intense bands in 900~1200 cm^{-1} region can be assigned to the typical stretching modes of CN heterocyclic. The intense band at 807cm^{-1} represented the out of plane breathing vibration characteristic of triazine unites.[37,38] And the peak at 3430cm^{-1} was attributed to the existence of water. For the $BiVO_4$/g-C_3N_4 composites, the peak intensities of ν_3 (VO_4) and ν_1 (VO_4) increased slightly with the increase of $BiVO_4$ content, indicating the co-existence of g-C_3N_4 and $BiVO_4$ in the composites.

The morphology of g-C_3N_4, $BiVO_4$ and 3:7 $BiVO_4$/g-C_3N_4 were investigated by SEM. From Fig. S1a, a structure with several stacking layers could be clearly seen in the g-C_3N_4 sample, which was in line with the literature reports.[39,40] The $BiVO_4$ sample displayed a plate-like structure with a diameter of 50 ~ 200 nm and a thickness of 10 ~ 30 nm (Fig. S1b). Fig. S1c revealed that the two types of materials were all found in the sample of $BiVO_4$/g-C_3N_4 with the molar ratio of 3:7. In addition, it was observed that quantities of $BiVO_4$ nanoparticles were clustered on or covered by the g-C_3N_4 nanosheets. In addition, the EDS profile in Fig. S1d and e clearly verified the presence of Bi, V, O, C, N elements in the 3:7 $BiVO_4$/g-C_3N_4 composite. The signal of Au was due to the gilding process.

The microstructure of g-C_3N_4, $BiVO_4$ and 3:7 $BiVO_4$/g-C_3N_4 were further investigated by TEM and HRTEM. Clearly, the two-dimensional layered structure of the pure g-C_3N_4 can be seen from Fig. 2a. Based on the crystal structure of g-C_3N_4 from theoretical and previously experimental work, it might be inferred that the top surface of the layer is the (002) facet of g-C_3N_4[23] as presented in Fig. 2d. As shown in Fig. 2b, the pure $BiVO_4$ shows a number of plate-like nanostructures with a thickness of 10 ~ 30 nm. Also, Fig. 2b and HRTEM (Fig. 2e) proved that the top surface of $BiVO_4$ is (121) facet. Fig. 2c displayed the two type of nanosheets attached to each other with (002) facets of g-C_3N_4 and (121) facets of $BiVO_4$, indicating that the coupling between g-C_3N_4 and $BiVO_4$ may happen on the (002) facets of g-C_3N_4 and (121) facets of $BiVO_4$

The XPS was employed to evaluate the surface chemical composition and the oxidation state of $BiVO_4$/g-C_3N_4 composites and to further study the interaction of g-C_3N_4 with $BiVO_4$. The overall XPS spectrum for the 3:7 $BiVO_4$/g-C_3N_4 was displayed in Fig. 3a, in which the Bi, O, V, C and N elements could all be investigated. Fig. 3b-f showed the high resolution spectra of Bi 4f, V 2p, O 1s, C 1s and N 1s for 3:7 $BiVO_4$/g-C_3N_4 composites, respectively. As shown in Fig. 3b, the binding energy values of Bi $4f_{7/2}$ and Bi $4f_{5/2}$ were observed at 164.4 eV and 159.1 eV, respectively. The high-resolution XPS spectra of 3:7 $BiVO_4$/g-C_3N_4 in Fig. 3c showed a peak at 529.5 eV, which can be attributed to V 2p. Obviously, two peaks can be detected in the high-resolution XPS spectra of O 1s region (Fig. 3d). And the main peak at 529.7 eV is assigned to the Bi-O bonds of $(Bi_2O_2)^{2+}$ slabs in the layered structure of $BiVO_4$, while the peak at 530.7eV is ascribed to the hydroxyl groups on the surface.[40] In Fig. 3e, the peak of C 1s at 284.6 eV is the characteristic of the

adventitious carbon on the surface of g-C_3N_4 and the peaks at 286 eV and 288.2 eV were both attributed to the sp^2 hybridized C (C-$(N)_3$).[10] The main features of N 1s are shown in Fig. 3f and a broad and wide peak (397 ~ 403 eV) can be seen. The existence of sp^2-bonded g-C_3N_4 in the $BiVO_4$/g-C_3N_4 composites could be verified by the N 1s peak at 398.8 eV reflecting the sp^2-hybridized nitrogen (C=N-C).[41] The two peaks observed at 400.1 eV and 401.3 eV were assigned to tertiary nitrogen (N-(C_3)) groups and the effects of charging reaction, respectively.[42] The XPS results further demonstrated that the $BiVO_4$/g-C_3N_4 composite was successfully obtained.

The UV-vis DRS of the composites were displayed in Fig. 4, from which the optical absorption edges of the pure g-C_3N_4 and $BiVO_4$ were approximately estimated from the absorption onsets to be 450 and 525 nm, respectively. After the combination of g-C_3N_4 and $BiVO_4$, the absorption band edges of the composites gradually shift toward that of pure $BiVO_4$ with the increase of $BiVO_4$ content, which reveals that $BiVO_4$ is a good and apposite visible-light sensitizer to g-C_3N_4. The band gap (Eg) can be determined by the formula:[43]

$$\alpha h\nu = A\,(h\nu - E_g)^{n/2} \quad (1)$$

Where α, h, m, E_g and A are absorption coefficient, Planck constant, light frequency, band gap energy, and a constant, respectively. Among them, n is determined by the type of optical transition of a semiconductor (n = 1 for direct transition and n = 4 for indirect transition).[44,45] As the previous literature reported, the n value of g-C_3N_4 was 4, and the n value of $BiVO_4$ was 1. From the plot of $(\alpha h\nu)^{1/2}$ or $(\alpha h\nu)^2$ versus (hv) in Fig. 4a and Fig. 4b, the E_g of g-C_3N_4 and $BiVO_4$ were estimated to be 2.60 eV and 2.45 eV, respectively. Meanwhile, the E_g of $BiVO_4$/g-C_3N_4 heterostructures were similar to that of pure $BiVO_4$.

3.2. Photocatalytic activity

The photocatalytic activity of the $BiVO_4$/g-C_3N_4 composite photocatalysts as well as pure $BiVO_4$ and C_3N_4 were examined by degradation of RhB molecules under visible-light irradiation (λ > 420 nm). Fig. 5a shows the photocatalytic degradation curves of RhB with the as-obtained photocatalysts under visible-light illumination for 5 h. It can be seen clearly that both the pristine g-C_3N_4 and $BiVO_4$ display relatively poor visible-light-induced degradation efficiency. When the molar ratio of $BiVO_4$ to g-C_3N_4 in the composites was 3:7, the highest degradation efficiency of 85% was observed within 5 h. The pseudo-first-order kinetic curves of RhB photodegradation were also plotted to analyze the degradation rate quantitatively. The experimental data clearly displayed that the apparent rate constant k is 0.033 h^{-1}, 0.032 h^{-1}, 0.066 h^{-1}, 0.139 h^{-1}, 0.342 h^{-1}, 0.041h^{-1}, and 0.049h^{-1} for the pristine g-C_3N_4, $BiVO_4$ and $BiVO_4$/g-C_3N_4 composites with molar ratios of 1:9, 2:8, 3:7, 4:6, 5:5, respectively (Fig. 5c). In other words, the photocatalytic activity of 3:7 $BiVO_4$/g-C_3N_4 is 10.36 and 10.68 times higher than those of single g-C_3N_4 and $BiVO_4$, respectively. From Fig. 5b, the maximum absorbance of the solution shifted from 554 to 530 nm after 5 h irradiation, indicating that the N-demethylation and de-ethylation reactions happened during the photodegradation process.[46,47] For the purpose of verifying the active species during the photocatalytic reaction and determining the corresponding photocatalytic mechanism,Tte tert-butyl alcohol (TBA), disodium ethylenediaminetetraacetate (EDTA) and 1, 4-benzoquinone (BQ) were employed as the hydroxyl radical (•OH) scavenger, hole (h^+) scavenger and superoxide radical ($\bullet O_2^-$) scavenger,[27] respectively. When EDTA was added to the solution, the RhB degradation rate for the 3:7 $BiVO_4$/g-C_3N_4 composite is slightly depressed as depicted in Fig. 5d, revealing that only a small amount of the holes were participated in the RhB degradation processes. However, the decrease of degradation rate is obviously observed with the addition of 1 mM of tertbutyl alcohol (TBA), which acted as a scavenger for •OH radical species. In addition, the degradation of RhB was also significantly depressed with adding 1 mM of $\bullet O_2^-$ scavenger BQ, indicating that the $\bullet O_2^-$ also play a vital role during the RhB oxidation process. Thus, the active species trapping experiments demonstrated that the $\bullet O_2^-$ and •OH are the two main active species in the degradation process of RhB. For the sake of comparison, the influences of additions (EDTA, TBA and BQ) toward the photocatalytic activity over both pure $BiVO_4$ and g-C_3N_4 were also investigated as illustrated in Fig. S2. From Fig. S2, we can conclude that $\bullet O_2^-$ plays the most crucial role in the oxidation process of RhB over pure g-C_3N_4. While for the pure $BiVO_4$, h^+ was the main active species in the RhB degradation process. Comparatively, as depicted in the Fig. 5d, the main active species of 3:7 $BiVO_4$/g-C_3N_4 sample in the degradation process of RhB are $\bullet O_2^-$ and •OH, which was in agreement with the principle of Z-scheme photocatalytic mechanism. The BET specific surface area of 3:7 $BiVO_4$/g-C_3N_4 composite is 4.52 m^2/g, which is a little higher than bulk g-C_3N_4 (4.01 m^2/g), indicating that the slightly increased specific surface area is not the main reason for the highly enhanced photocatalytic activity of $BiVO_4$/g-C_3N_4 composite.

3.3. Mechanism investigation on the enhanced photocatalytic activity

The conduction band (CB) and valence band (VB) potentials of g-C_3N_4 and $BiVO_4$ can be calculated by the following equations:[48]

$$E_{VB} = X - E_e + 0.5E_g \quad (2)$$

$$E_{CB} = E_{VB} - E_g \quad (3)$$

where E_{VB} is the VB edge potential; X is the electronegativity of the semiconductor, which is the geometric average of the absolute electronegativity of the constituent atoms (X values of g-C_3N_4 and $BiVO_4$ are 4.67eV and 6.16eV, respectively); E_e is the energy of free electrons on the hydrogen scale ($E_e \approx 4.5$ eV);[49] and E_g is the band gap energy of the semiconductor. The band gap energies of g-C_3N_4 and $BiVO_4$ are adopted as 2.60 eV and 2.45 eV, respectively. The positions of the conduction and the valence bands of g-C_3N_4 and $BiVO_4$ calculated by Eq. (2) and (3) were listed in Table S1 (Supporting Information).

Fig. 6a depicts the crystal structure of $BiVO_4$, which is a typical scheelite compound. Its crystal structure is composed of alternating $(Bi_2O_2)^{2+}$ slabs and $(VO_4)^{2-}$ octahedral layers. This layered configuration is considered to enhance the separation of electron-hole pairs and decrease the recombination rate of the charge carriers. The (121) facet of $BiVO_4$ was figuratively marked in the Fig. 6a. The two types of nanosheets attached to

each other with (002) facets of g-C_3N_4 and (121) facets of $BiVO_4$. Thus, we can deem that the coupled structure between g-C_3N_4 and $BiVO_4$ will benefit for the separation of electron-hole pairs, so as to contribute to the enhancement of photodegration on RhB under visible-light irradiation. The possible separation and transfer mechanism of the photoexcited charge carriers was proposed as depicted in Fig. 6c. Because the gap (1.56eV) between the CB of g-C_3N_4 and the CB of $BiVO_4$ is much larger than that (1.04eV) between the CB of $BiVO_4$ and the VB of g-C_3N_4, the photoexcited electrons in the CB of $BiVO_4$ transfer to the VB of g-C_3N_4 quickly, leading to the combination of electrons in the CB of $BiVO_4$ and photogenerated holes in the VB of g-C_3N_4. It accumulated rich electrons in the CB of g-C_3N_4 and holes in the VB of $BiVO_4$ to involve in the redox reactions. Consequently, the more negative potentiated electrons in the CB of g-C_3N_4 reduce the molecular oxygen to yield $\bullet O_2^-$, and then induces the RhB degradation. Meanwhile, the more positive potentiated holes in the VB of $BiVO_4$ produce rich active •OH radicals with powerful oxidization. Hence the photocatalytic activity of $BiVO_4$/g-C_3N_4 composites were significantly promoted, and RhB is photodegraded via $\bullet O_2^-$, •OH or direct h^+ oxidation pathway. Based on the above results, the $BiVO_4$/g-C_3N_4 system is a type of direct Z-scheme photocatalyst.

In order to prove the mechanism responsible for the remarkably improved visible-light induced photocatalysis, we conducted a series of tests such as photoluminescence spectra (PL), photocurrent-time measurement and electrochemical impedance spectroscopy (EIS).[50-52] PL emissionare mainly originated from the recombination of the photoexcited electrons and holes in semiconductors. And PL intensity has a strong correlation with photocatalytic activity of a photocatalyst. Generally, lower PL intensity reveals lower recombination rate of electron-hole pairs, thus higher photocatalytic performance.[26,53] In order to analyze the recombination of the charge carriers generated from g-C_3N_4, $BiVO_4$, and 3:7 $BiVO_4$/g-C_3N_4, the PL spectra with excitation wavelength 254 nm were measured and depicted in Fig. 7. The main emission peak centred on 460 nm for the g-C_3N_4 sample could be attributed to the band gap recombination of charge carries. In comparison with g-C_3N_4, combining with $BiVO_4$ does not affect the spectral position of the peaks, but reduces the relative intensity of PL spectra (inset of the Fig. 7). These results indicated that the mediator-free direct Z-scheme photocatalytic system of $BiVO_4$/g-C_3N_4 dedicates to the effective charge separation, thus creating a significantly improved photocatalytic activity for the $BiVO_4$/g-C_3N_4 composites under visible-light irradiation.

The photocurrent-time measurement was employed to evaluate the interfacial charge transfer dynamics between the g-C_3N_4 and $BiVO_4$. Fig. 8a displays the transient photocurrent responses produced by the pure g-C_3N_4, $BiVO_4$ and 3:7 $BiVO_4$/g-C_3N_4 samples. The photocurrent intensity remained at a relatively high constant value when the light was on and rapidly decreased to zero as long as the light was turned off. Obviously, the photocurrent over 3:7 $BiVO_4$/g-C_3N_4 composite is greatly improved, which is about 2 and 3 times as those of $BiVO_4$ and g-C_3N_4, respectively. The higher photocurrent demonstrates the higher efficiency of charge separation.[27,54] The results of photocurrent-time measurement suggested that the 3:7 $BiVO_4$/g-C_3N_4 heterostructure possesses more powerful ability in charge separation than the pristine g-C_3N_4 and $BiVO_4$. EIS measurement was employed to detect the charge transfer processes at solid/electrolyte interfaces. The radius of the arc on the EIS spectra implies the interface layer resistance happened on the surface of electrode. The smaller arc radius indicates the higher efficiency of charge transfer.[26,27,46] As shown in Fig. 8b, the diameter of the arc radius on the EIS Nynquist plot of the 3:7 $BiVO_4$/g-C_3N_4 composite electrode is much smaller than that of the pure $BiVO_4$ electrode, suggesting a more effective separation of photoexcited charge carries and rapid interfacial charge transfer occurred in the 3:7 $BiVO_4$/g-C_3N_4 composites.

To further confirm the Z-scheme mechanism and examine that the $\bullet O_2^-$ and •OH radicals mainly conduce to the degradation of RhB molecules over 3:7 $BiVO_4$/g-C_3N_4 under visible light irradiation ($\lambda > 420$ nm). Quantification experiments of $\bullet O_2^-$ production were performed thorough the transformation of NBT (detection agent of $\bullet O_2^-$) during the photocatalytic reaction.[23] Fig. 9 showed the spectra of the transformation percentage of NBT. For pure g-C_3N_4, the CB potential of g-C_3N_4 (–1.13 eV vs NHE) is more negative than E_0 ($O_2/\bullet O_2^-$ = –0.046 eV vs NHE). Thus, g-C_3N_4 shows obvious transformation percentage of NBT (Fig. 9a), while that for pure $BiVO_4$ (Fig. 9b) can be neglected. It can be concluded that there are almost no $\bullet O_2^-$ produced from the electrons of $BiVO_4$, because its CB potential (0.43 eV vs NHE) is more positive than E_0 ($O_2/\bullet O_2^-$ = –0.046 eV vs NHE), and the standard redox potential of Bi^{4+}/Bi^{3+} (1.59 eV) is more negative than that of $\bullet OH/OH^-$ (+1.99 eV).[27] After the combination of g-C_3N_4 and $BiVO_4$, most of electrons in the CB of $BiVO_4$ were transferred to the VB of g-C_3N_4 and recombined with the holes there according to the above energy potentials analysis (Fig. 6), which enables the electrons remained in the CB of g-C_3N_4 to react with O_2 to generate more $\bullet O_2^-$. It was proved by the highest transformation percentage of NBT of $BiVO_4$/g-C_3N_4 as shown in Fig. 9c. Moreover, the NBT transformation percentage of the 3:7 $BiVO_4$/g-C_3N_4 composite is also higher than that of the mechanically mixed sample (Fig. 9d). These results demonstrate that the photogenerated electrons on the CB of $BiVO_4$ could easily transfer to the VB of g-C_3N_4, resulting in more effective charge separation and reducing the probability of recombination of electron-hole pairs in the $BiVO_4$/g-C_3N_4 composites. Especially, the 3:7 $BiVO_4$/g-C_3N_4 holds more g-C_3N_4, leading to that more photogenerated electrons can react with O_2 to produce $\bullet O_2^-$ and take part in decomposition of RhB, which is in good agreement with the active species trapping experiments (Fig 5d).

Furthermore, the terephthalic acid photoluminescence probing technique (TA-PL) was also applied to investigate the •OH radicals since TA could react with •OH radicals to from a highly fluorescent 2-hydroxyterephthalic acid (TAOH).[30,50] For pure $BiVO_4$, there is almost no •OH species generated because of the rapid decay through recombination of photoexcited charge carries (Fig. 10b). Compared with pure g-C_3N_4 (Fig. 10a) and $BiVO_4$(Fig. 10b), the highest PL intensity was observed over the 3:7 $BiVO_4$/g-C_3N_4 composite as shown in Fig. 10c. This should be attributed to the Z-scheme charge transfer,[27,29] which results in the enrichment of holes on the VB of $BiVO_4$ to produce more

•OH, resulting in the highest PL peak of $BiVO_4$/g-C_3N_4 composite. In addition, the PL intensities of $BiVO_4$/g-C_3N_4 composite at approximately 425 nm at different times in Fig. 10c were also obviously higher than that of the mechanically mixed sample (Fig. 10d), confirming the successful construction of $BiVO_4$/g-C_3N_4 composite with efficient charge transfer. Based on the results of NBT transformation and TA-PL results, the photodecomposition of RhB over $BiVO_4$/g-C_3N_4 is truly according to a Z-scheme reaction mechanism.

4. Conclusions

A mediator-free direct Z-scheme photocatalyst $BiVO_4$/g-C_3N_4 was synthesized via a mixed-calcinations route. The coupling between g-C_3N_4 and $BiVO_4$ happens on the (002) and (121) facets of g-C_3N_4 and $BiVO_4$, respectively. All the as-synthesized $BiVO_4$/g-C_3N_4 composites exhibited more excellent photocatalytic performance than the individuals under visible-light irradiation. The detailed active species trapping and quantification experiments of $\bullet O_2^-$ and •OH production over $BiVO_4$/g-C_3N_4 composites and the individuals revealed that the significantly improved photocatalytic activity should be attributed to the fabrication of Z-scheme principled $BiVO_4$/g-C_3N_4, which can result in the more efficient separation and largely reduced recombination probability of photoexcited electron-hole pairs, thus enabling highly powerful oxidation and reduction capability. It was also verified by the PL spectra and photoelectrochemical experiments.

Acknowledgement

This work was supported by the National Natural Science Foundations of China (Grant No. 51302251, 51172245), the Fundamental Research Funds for the Central Universities (2652013052), and the National High Technology Research and Development Program (863 Program 2012AA06A109) of China.

Notes and references

[a] *Beijing Key Laboratory of Materials Utilization of Nonmetallic Minerals and Solid Wastes, National Laboratory of Mineral Materials, School of Materials Science and Technology, China University of Geosciences, Beijing, 100083, China*
E-mail: hhw@cugb.edu.cn; zyh@cugb.edu.cn; Tel: 86-10-82332247.
[b] *Key Laboratory of Photochemical Conversion and Optoelectronic Materials, Technical Institute of Physics and Chemistry, Chinese Academy of Sciences, Beijing 100190, China*

† Electronic Supplementary Information (ESI) available: Absolute electronegativity, energy band gap, calculated conduction band edge position and valence band edge position of g-C_3N_4 and $BiVO_4$ semiconductors. SEM images of the g-C_3N_4, $BiVO_4$ and 3:7 $BiVO_4$/g-C_3N_4 samples. Photocatalytic degradation curves of RhB over g-C_3N_4 and $BiVO_4$ alone and with the addition of TBA, EDTA, or BQ. See DOI:10.1039//b000000x

1 A. Fujishima and K. Honda, *Nature.* 1972, 238, 37.
2 L. Shang, T. Bian, B. Zhang, D. H. Zhang, L. Z. Wu, C. H. Tung, Y. D. Yin and T. R. Zhang, *Angew. Chem., Int. Ed.* 2014, 53, 250.
3 J. G. Yu, J. X. Low, W. Xiao, P. Zhou and M. Jaroniec, *J. Am. Chem. Soc.* 2014, 136, 8839.
4 X. J. Lang, W. R. Leow, J. C. Zhao, and X. D. Chen, ChenChem. Sci. 2014, 10.1039/C4SC02891k.
5 X. T. Wang, C. H. Liow, D. P. Qi, B. W. Zhu, W. R. Leow, H. Wang, C. Xue, X. D. Chen, and S. Z. Li, *Adv. Mater.* 2014, 26, 3506.
6 X. J. Lang, X. D. Chen, and J. C. Zhao, *Chem. Soc. Rev.* 2014, 43, 473.
7 Y. Y. Zhang, Y. X. Tang, X. F. Liu, Z. L. Dong, H. H. Hng, Z. Chen, T. C. Sum, and X. D. Chen, *Small.* 2013, 9, 996.
8 P. Zhou, J. G. Yu and M. Jaroniec, *Adv. Mater.* 2014, DOI: 10.1002/adma. 201400288.
9 J. G. Yu, S. H. Wang, J. X. Low and W. Xiao, *Phys. Chem. Chem. Phys.*, 2013, 15, 16883.
10 Y. X. Yang, W. Guo, Y. N. Guo, Y. H. Zhao, X. Yuan and Y. H. Guo, *J. Hazard. Mater.* 2014, 271, 150.
11 X. F. Wang, S. F. Li, Y. Q. Ma, H. G. Yu and J. G. Yu, *J. Phys. Chem. C.* 2011, 115, 14648.
12 L. Ding, H. Zhou, S. Lou, J. Ding, D. Zhang, H. X. Zhu and T. X. Fan, *Int. J. Hydrogen Energ.* 2013, 38, 8244.
13 J. G. Hou, Z. Wang, C. Yang, W. L. Zhou, S. Q. Jiao and H. M. Zhu, *J. Phys. Chem. C.* 2013, 117, 5132.
14 X. W. Wang, G. Liu, Z. G. Chen, F. Li, L. Z. Wang, G. Q. Lu and H. M. Cheng, *Chem. Commun.* 2009, 3452.
15 H. J. Yun, H. J. Lee, N. D. Kim, D. M. Lee, S. J. Yu and J. H. Yi, *Acs Nano.* 2011, 5, 4084.
16 M. Miyauchi, Y. Nukui, D. Atarashi and E. Sakai, *Appl. Mater. Interfaces.* 2013, 5, 9770.
17 Maeda, K. *ACS Catal.* 2013, 3, 1486.
18 L. Ge, C. C. Han, and J. Liu, *J. Mater. Chem.* 2012, 22, 11843.
19 L. Ge, C. C. Han, X. L. Xiao, L. L. Guo, *Int. J. Hydro. Energy.* 2013, 38, 6960.
20 C. C. Hana, L. Ge, C. F. Chen, Y. J. Li, X. L. Xiao, Y. N. Zhang, L. L. Guo, *Appl. Catal. B: Environ.* 2014, 147, 546.
21 F. Dong, Z. Y. Wang, Y. H. Li, W. K. Ho and S. C. Lee, *Environ. Sci. Technol.* 2014, 48, 10345.
22 G. Liu, P. Niu, C. Sun, S. C. Smith, Z. Chen, G. Q. Lu and H. M. Cheng, *J. Am. Chem. Soc.* 2010, 132, 11642.
23 L. Q. e, J. Y. Liu, Z. Jiang, T. Y. Peng and L. Zan, *Appl. Catal. B: Environ.* 2013, 142-143, 1.
24 W. Z. Wang, X. W. Huang, S. Wu, Y. I. Zhou, L. G. Wang, H. L. Shi, Y. J. Liang and B. Zou, *Appl. Catal. B: Environ.* 2013, 134-135, 293.
25 H. W. Huang, S. B. Wang, N. Tian and Y. H. Zhang, *Rsc Adv.* 2014, 4, 5561.
26 J. Fu, B. Chang, Y. Tian, F. Xi and X. Dong, *J. Mater. Chem. A.* 2013, 1, 3083.
27 T. Xu, L. Zhang, H. Cheng, Y. Zhu, *Appl. Catal. B: Environ.* 2011, 101, 382.
28 S. F. Chen, Y. F. Hu, S. G. Meng and X. L. Fu, *Appl. Catal. B: Environ.* 2014, 150, 564.
29 S. F. Chen, Y. F. Hu, L. Ji, X. L. Ji and X. L. Fu, *Appl. Surf. Sci.* 2014, 292, 357.
30 K. I. Ishibashi, A. Fujishima, T. Watanab and K. Hashimoto, *Electrochem. Commun.* 2000, 2, 207.
31 Z. D. Wu, L. L. Chen, C. S. Xing, D. L. Jiang, J. M. Xie and M. Chen, *Dalton T.* 2013, 42, 12980.
32 M. R. Hoffmann, S. T. Martin, W. Choi and D. M. Bahnemann, *Chem. Rev.* 1995, 95, 69.
33 F. Dong, T. Xiong, Y. J. Sun, Z. W. Zhao, Y. Zhou, X. Feng, Z. B. Wu, *Chem. Commun.* 2014, 50, 10386.
34 H. F. Lai, C. C. Chen, Y. K. Chang, C. H. Lu and R. G. Wu, *Sep. Purif. Technol.* 2014, 122, 78.
35 R. L. Frost, D. A. Henry, M. L. Weier and W. Martens, *J. Raman Spectrosc.* 2006, 37, 722.
36 J. Cao, C. C. Zhou, H. L. Lin, B. Y. Xu and S. F. Chen, *Appl. Surf. Sci.* 2013, 284, 263.
37 G. Zhang, J. Zhang, M. Zhang and X. Wang, *J. Mater. Chem.* 2012, 22, 8083.
38 J. Liu, T. Zhang, Z. Wang, G. Dawson and W. Chen, *J. Mater. Chem.* 2011, 21, 14398.
39 X. J. Wang, Q. Wang, F. T. Li, W. Y. Yang, Y. Zhao, Y. J. Hao and S. J. Liu, *Chem. Eng. J.* 2013, 234, 361.
40 Z. H. Ai, W. K. Ho, S. C. Lee and L. Z. Zhang, *Environ. Sci. Technol.* 2009, 43, 4143.
41 S. C. Yan, Z. S. Li, Z. G. Zou, *Langmuir.* 2010, 26, 3894.

42 H. H. Ji, F. Chang, X. F. Hua, W. Qin, J. W. Shen, *Chem. Eng. J.* 2013, 218, 183.

43 H. W. Huang, L. J. Liu, S. F. Jin, W. J. Yao, Y. H. Zhang and C. T. Chen, *J. Am. Chem. Soc.* 2013, 135, 18319.

44 W. S. Kuo and P. H. Ho, *Dyes Pigments.* 2006, 71, 212.

45 H. W. Huang, Y. He, Z. S. Lin, L. Kang and Y. H. Zhang, *J. Phys. Chem. C.* 2013, 117, 22986.

46 A. Fujishima, T. N. Rao and T. A. Tryk, *J. Photochem. Photobiol. C:Photochem. Rev.* 2000, 1, 1.

47 F. Duan, Y. Zheng and M. Q. Chen, *Appl. Surf. Sci.* 2011, 257, 1972.

48 W. R. Zhao, Y. Wang, Y. Yang, J. Tang and Y. Yang, *Appl. Catal. B: Environ.* 2012, 115-116, 90.

49 H. W. Huang, J. Y. Yao, Z. S. Lin, X. Y. Wang, R. He, W. J. Yao, N. X. Zhai and C. T. Chen, *Angew. Chem. Int. Ed.* 2011, 50, 9141.

50 Y. M. He, J. Cai, T. T. Li, Y. Wu, H. J. Lin, L. H. Zhao and M. F. Luo, *Chem. Eng. J.* 2013, 215-216, 721.

51 G. P. Dai, J. G. Yu, G. Liu, *J. Phys. Chem. C.* 2011, 115, 7339.

52 X. J. Bai, L. Wang, R. L. Zong, Y. H. Lv, Y. Q. Sun and Y. F. Zhu, *Langmuir.* 2013, 29, 3097.

53 M. Yang, Q. Huang and X. Q. Jin, *Mater. Sci. Eng. B.* 2012, 177, 600.

54 H. W. Huang, K. Liu, K. Chen, Y. L. Zhang, Y. H. Zhang and S. C. Wang, *J. Phys. Chem. C* 2014, 118, 14379.

Cite this: DOI: 10.1039/c0xx00000x

www.rsc.org/xxxxxx

ARTICLE TYPE

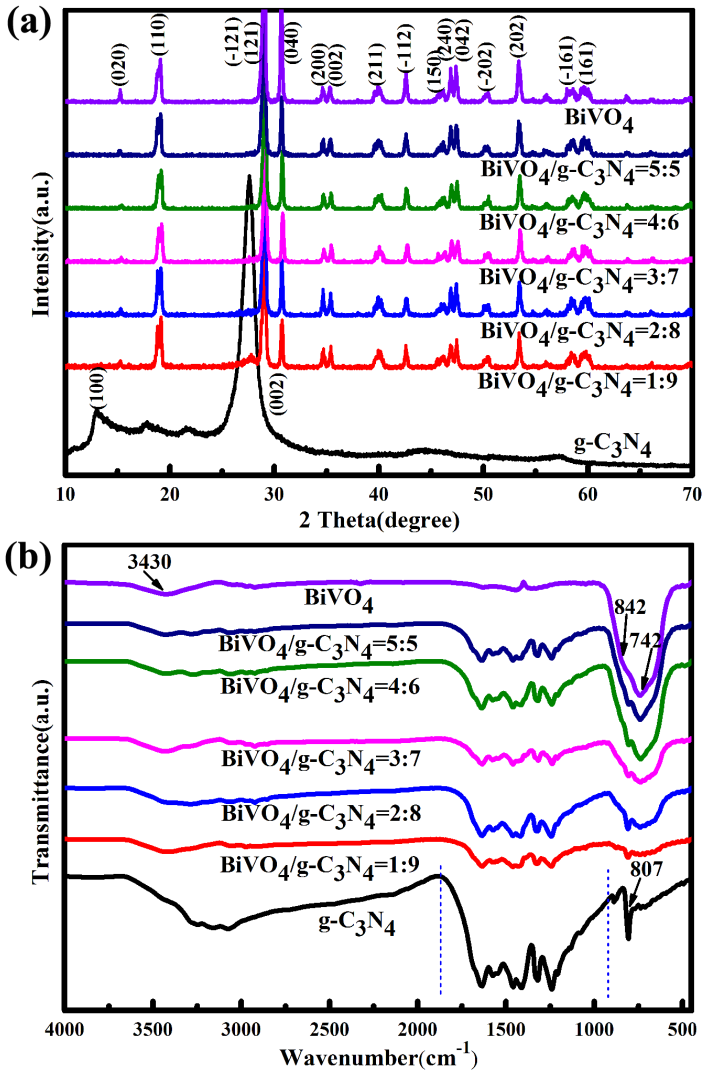

Fig. 1 (a) XRD patterns and (b) FTIR spectra of g-C_3N_4, $BiVO_4$ and $BiVO_4$/g-C_3N_4 composites with molar ratios of 1:9, 2:8, 3:7, 4:6 and 5:5.

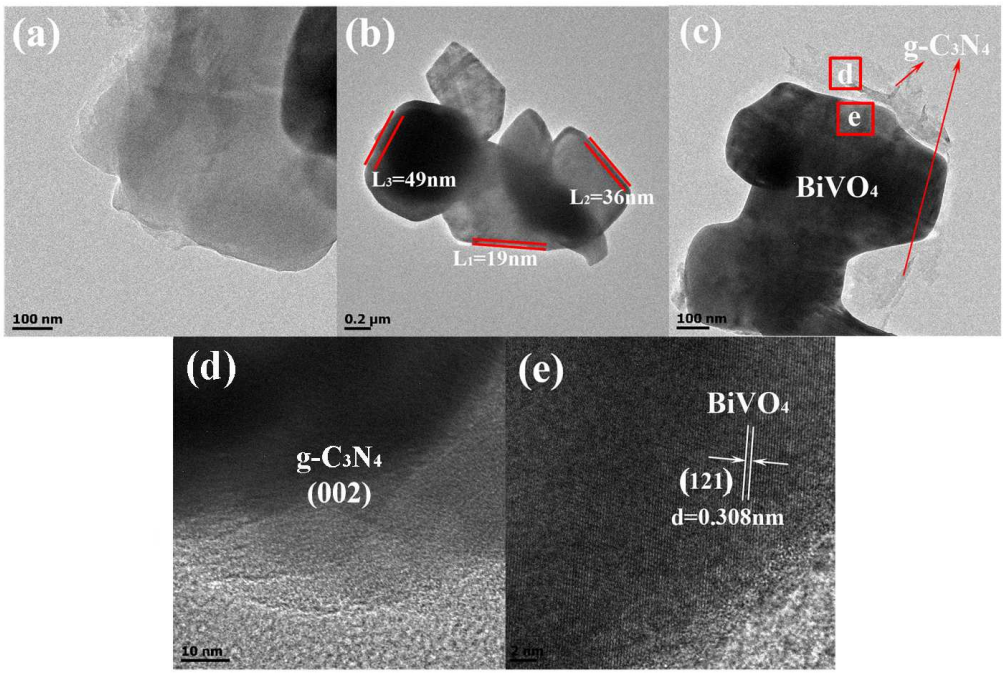

Fig. 2 TEM images of the as-obtained samples: (a) g-C_3N_4, (b) $BiVO_4$, (c) 3:7 $BiVO_4$/g-C_3N_4; HRTEM images of (d, e) 3:7 $BiVO_4$/g-C_3N_4.

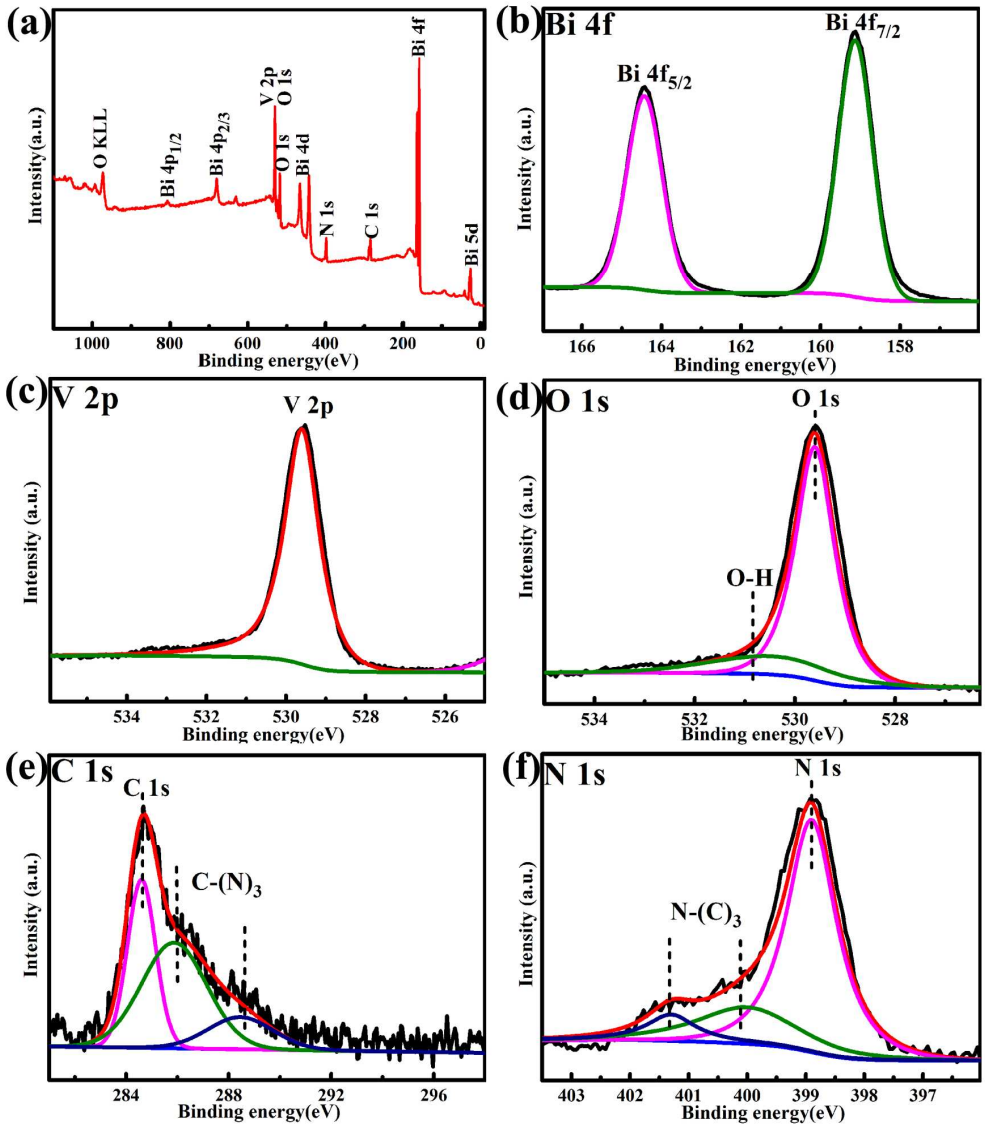

Fig. 3 (a) Typical XPS survey spectra of 3:7 $BiVO_4$/g-C_3N_4. High resolution XPS spectra of (b) Bi 4f, (c) V 2p, (d) O 1s, (e) C 1s, and (f) N 1s of 3:7 $BiVO_4$/g-C_3N_4.

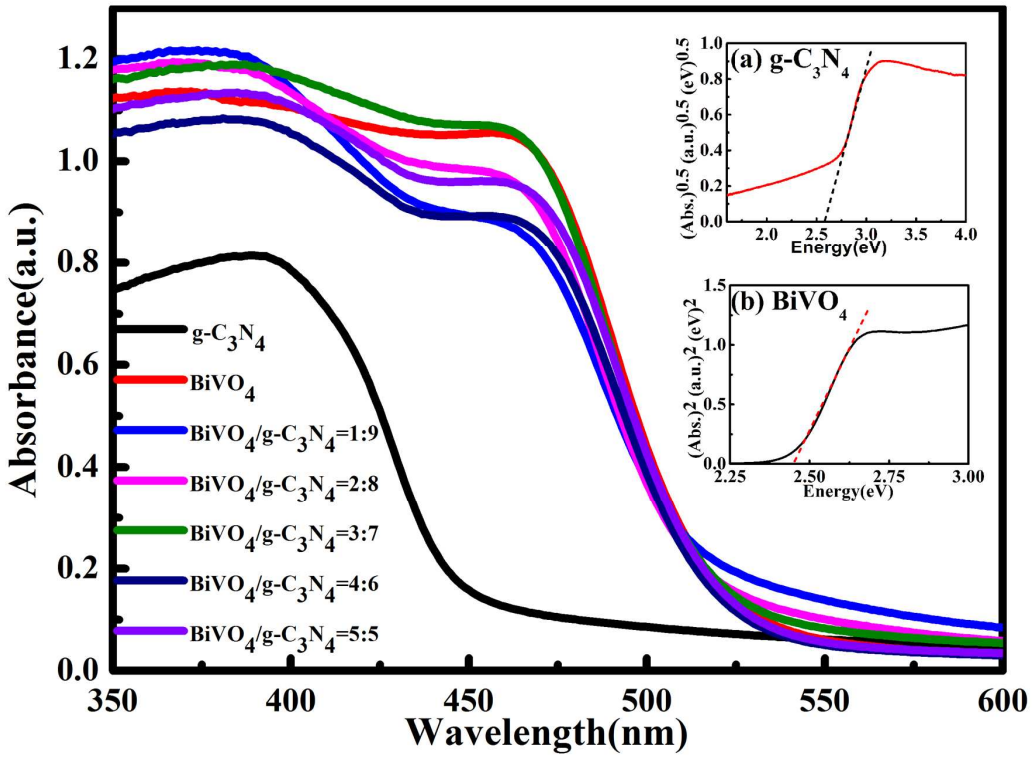

Fig. 4 UV-vis diffuse reflectance spectra of g-C_3N_4, $BiVO_4$, $BiVO_4$/g-C_3N_4 composites with molar ratios of 1:9, 2:8, 3:7, 4:6 and 5:5.

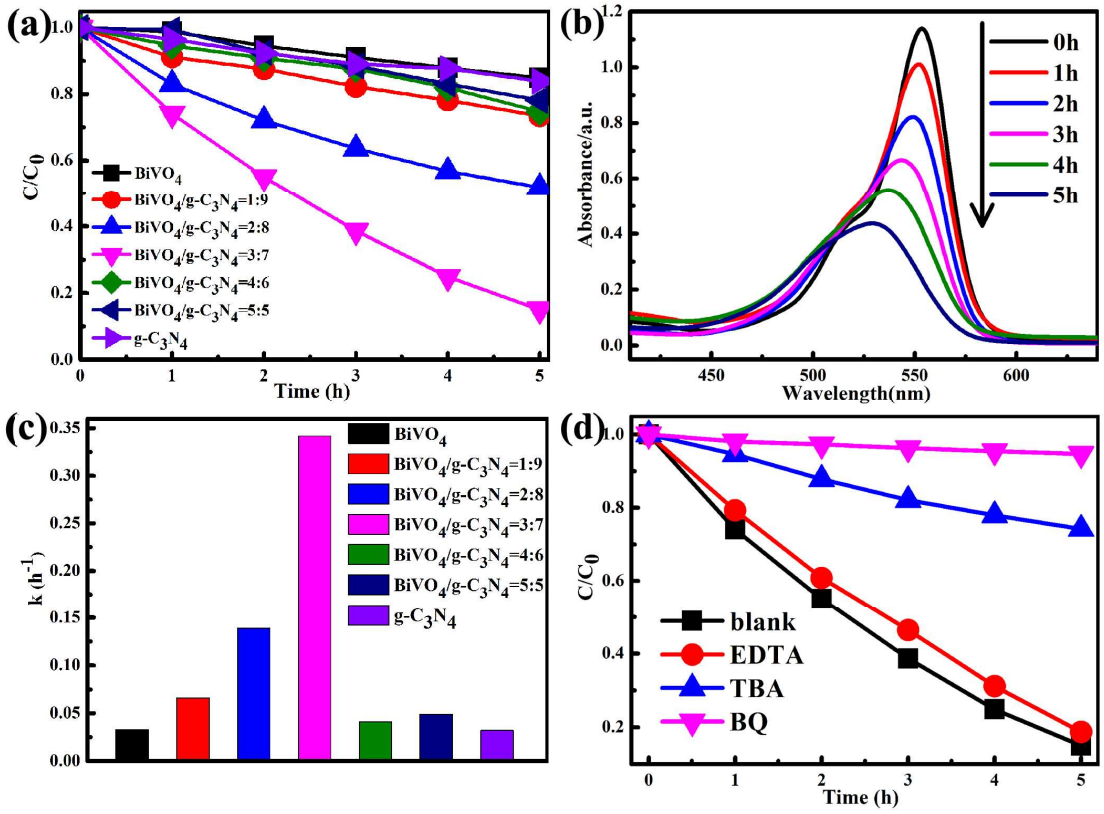

Fig. 5 (a) Photocatalytic degradation curves of RhB over as-prepared $BiVO_4/g\text{-}C_3N_4$ samples under the visible light irradiation ($\lambda > 420$ nm); (b) UV−visible spectra of RhB at different visible-irradiation-times in the presence of 3:7 $BiVO_4/g\text{-}C_3N_4$; (c) Apparent rate constants for the photodegradation of RhB over $BiVO_4/g\text{-}C_3N_4$ under visible light irradiation ($\lambda > 420$ nm); (d) Photocatalytic degradation of RhB over 3:7 $BiVO_4/g\text{-}C_3N_4$ photocatalysts alone and with the addition of TBA, EDTA, or BQ.

Cite this: DOI: 10.1039/c0xx00000x

www.rsc.org/xxxxxx

ARTICLE TYPE

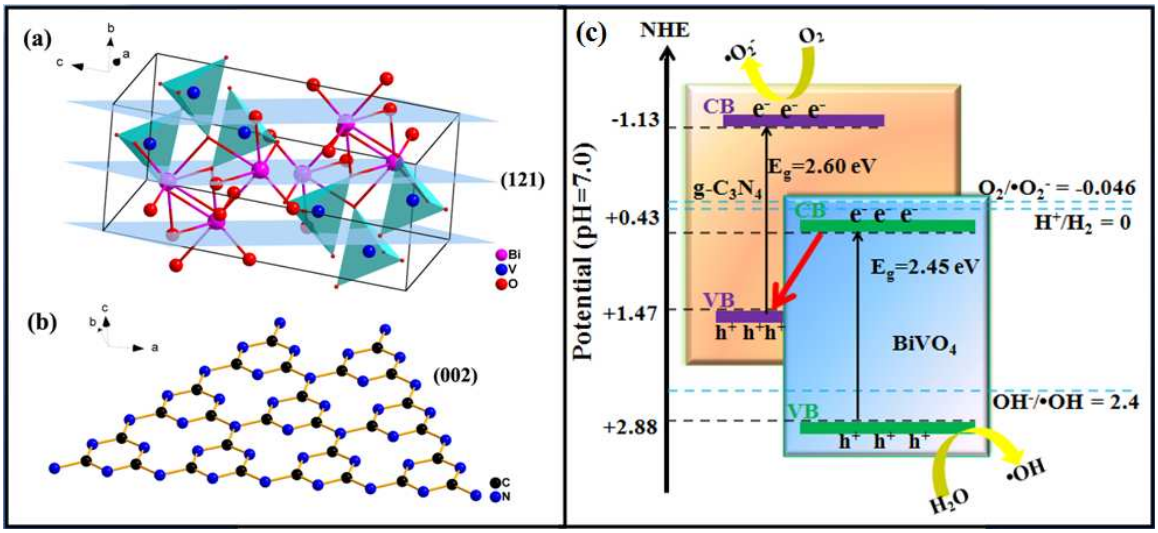

Fig. 6 Crystal structure of (a) $BiVO_4$ and (b) g-C_3N_4; (c) Schematic diagrams for interfacial charge transfer of $BiVO_4$/g-C_3N_4 Z-scheme photocatalyst.

Cite this: DOI: 10.1039/c0xx00000x

www.rsc.org/xxxxxx

ARTICLE TYPE

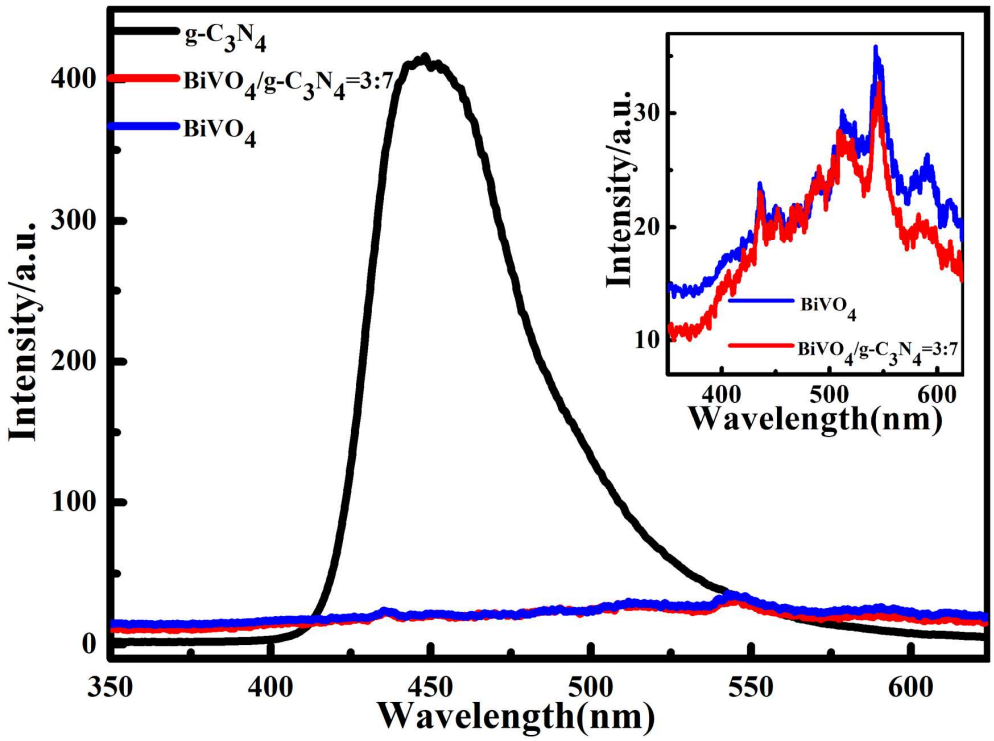

Fig. 7 Photoluminescence spectra of g-C_3N_4, $BiVO_4$, and 3:7 $BiVO_4$/g-C_3N_4 photocatalysts.

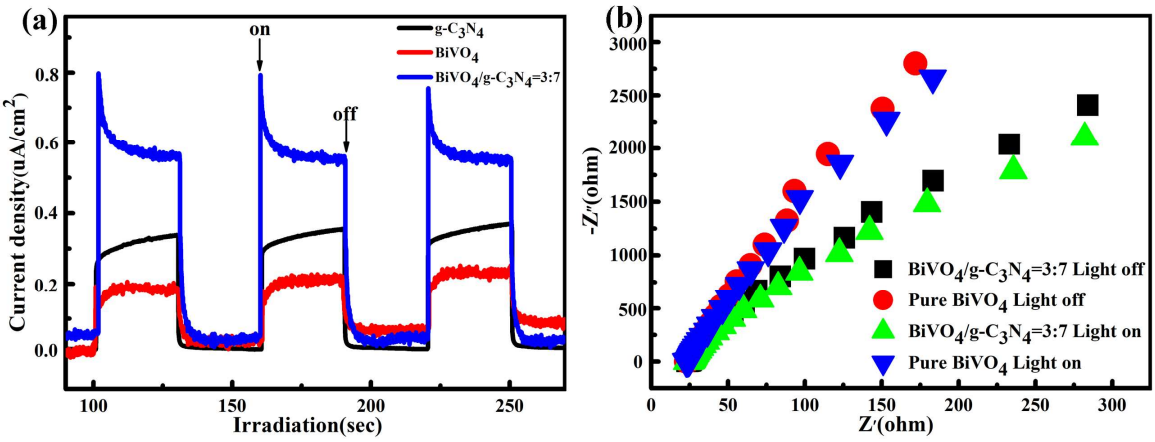

Fig. 8 (a) Comparison of transient photocurrent responses of the g-C_3N_4, $BiVO_4$ and 3:7 $BiVO_4$/g-C_3N_4 and (b) EIS Nynquist plots of the g-C_3N_4 and 3:7 $BiVO_4$/g-C_3N_4 with light on/off cycles under visible light irradiation ($\lambda > 420$ nm, [Na_2SO_4] = 0.1 M).

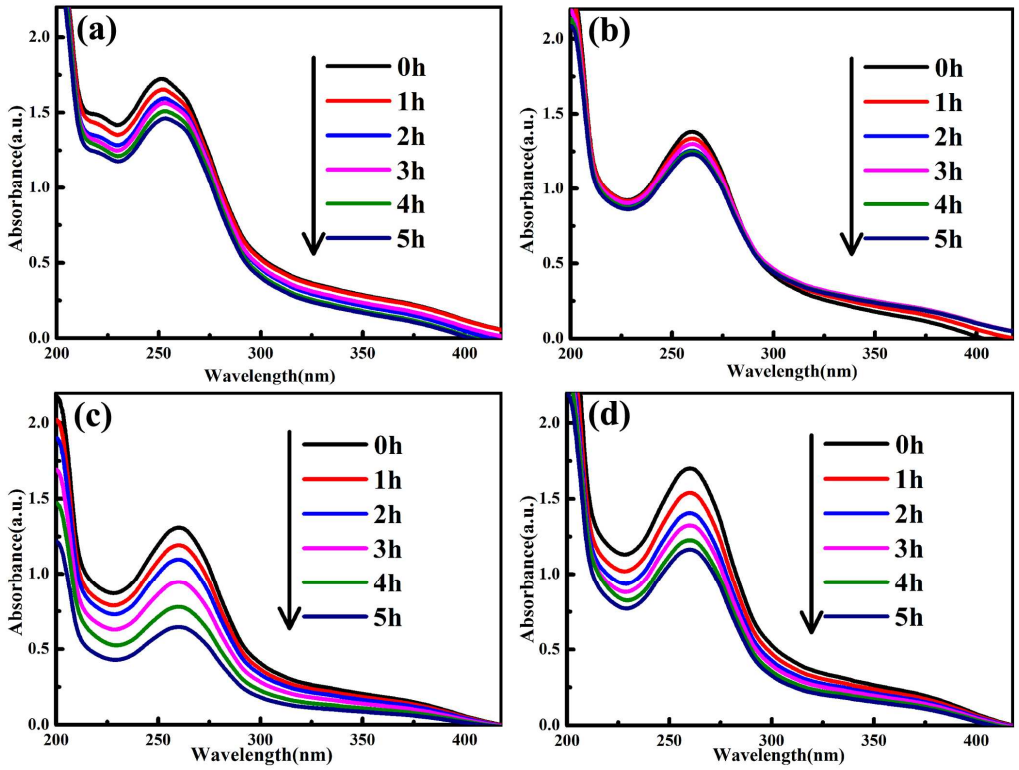

Fig. 9 Spectra of NBT transformation generated by (a) 50mg of g-C_3N_4, (b) 50mg of $BiVO_4$, (c) 50mg of 3:7 $BiVO_4$/g-C_3N_4 and (d) mechanically mixed 35mg g-C_3N_4 with 15mg $BiVO_4$ under irradiation with visible light ($\lambda > 420$ nm).

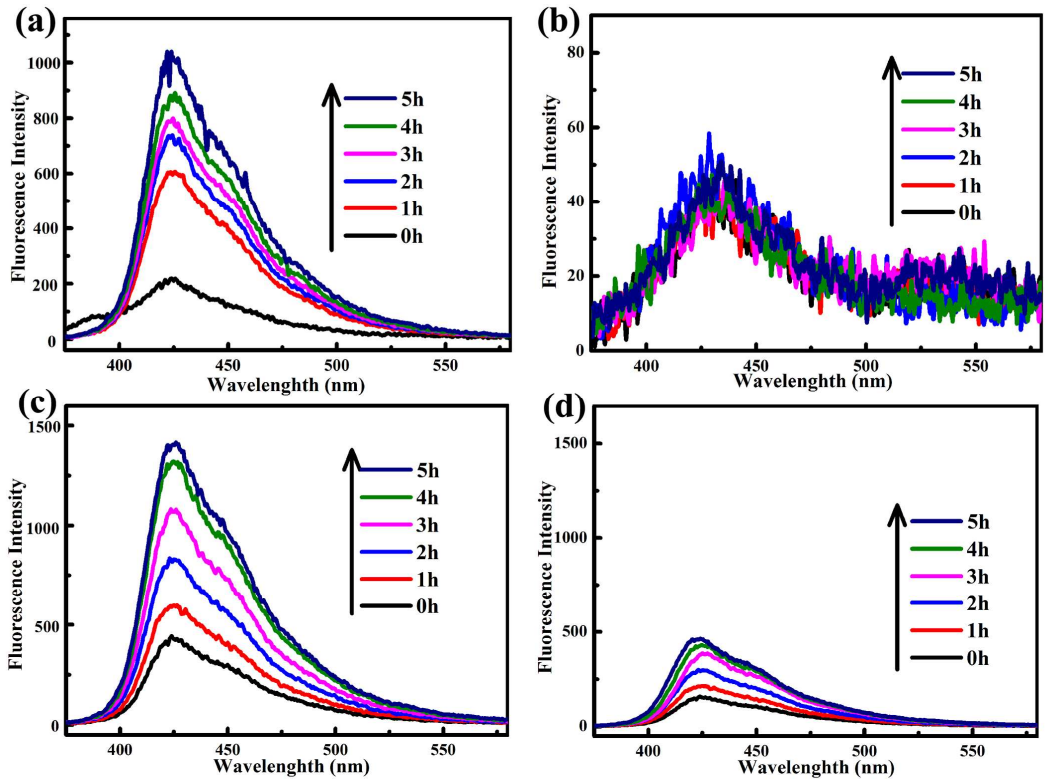

Fig. 10 Fluorescence spectra of a TAOH solution generated by (a) 50mg of g-C_3N_4, (b) 50mg of $BiVO_4$, (c) 50mg of 3:7 $BiVO_4$/g-C_3N_4 and (d) mechanically mixed 35mg g-C_3N_4 with 15mg $BiVO_4$ under irradiation with visible light ($\lambda > 420$ nm)

Cite this: DOI: 10.1039/c0xx00000x

www.rsc.org/xxxxxx

ARTICLE TYPE

Mediator-free direct Z-scheme photocatalytic system: $BiVO_4$/g-C_3N_4 organic-inorganic hybrid photocatalyst with highly efficient visible-light-induced photocatalytic activity

Na Tian[a], Hongwei Huang[a]*, Ying He [a], Yuxi Guo [a], Tieriu Zhang [b], Yihe Zhang [a]*

[a] *Beijing Key Laboratory of Materials Utilization of Nonmetallic Minerals and Solid Wastes, National Laboratory of Mineral Materials, School of Materials Science and Technology, China University of Geosciences, Beijing, 100083, China*

[b]*Key Laboratory of Photochemical Conversion and Optoelectronic Materials, Technical Institute of Physics and Chemistry, Chinese Academy of Sciences, Beijing 100190, China*

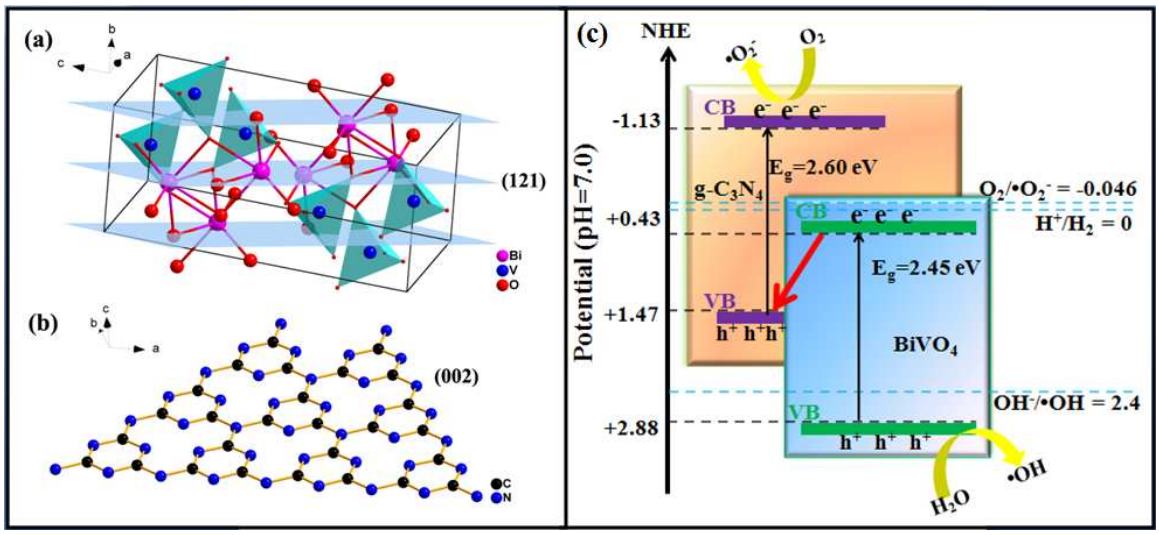

Mediator-free Z-scheme $BiVO_4$/g-C_3N_4 photocatalysts were successfully obtained based on band gap engineering design. It exhibits high visible-light-driven photocatalytic activity for degradation of RhB and photocurrent generation. The much more powerful oxidation and reduction capability of the samples were demonstrated by the active species experiments, NBT transformation and TA-PL probing technique.